Published in final edited form as:
Science. ; 369(6508): . doi:10.1126/science.aaz7714.

Reconstitution of autophagosome nucleation defines Atg9 vesicles as seeds for membrane formation

Justyna Sawa-Makarska[1,*,#], **Verena Baumann**[1,*], **Nicolas Coudevylle**[1,*], **Sören von Bülow**[2], **Veronika Nogellova**[1], **Christine Abert**[1], **Martina Schuschnig**[1], **Martin Graef**[3], **Gerhard Hummer**[2,4], **Sascha Martens**[1,#]

[1]Department of Biochemistry and Cell Biology, Max Perutz Labs, University of Vienna, Dr. Bohr-Gasse 9/5, 1030 Vienna, Austria

[2]Department of Theoretical Biophysics, Max Planck Institute of Biophysics, Max-von-Laue Straße 3, 60438, Frankfurt am Main, Germany

[3]Max Planck Institute for Biology of Ageing, 50931 Cologne, Germany; CECAD, University of Cologne, 50931 Cologne, Germany

[4]Institute for Biophysics, Goethe University Frankfurt, 60438 Frankfurt am Main, Germany

Abstract

Autophagosomes form de novo in a manner that is incompletely understood. Particularly enigmatic are Atg9 containing vesicles that are required for autophagy machinery assembly but do not supply the bulk of the autophagosomal membrane. Here we reconstituted autophagosome nucleation using recombinant components from yeast. We found that Atg9 proteoliposomes first recruited the phosphatidylinositol 3-phosphate kinase complex, followed by Atg21, the Atg2-Atg18 lipid transfer complex and the E3-like Atg12–Atg5-Atg16 complex, which promoted Atg8 lipidation. Furthermore, we found that Atg2 could transfer lipids for Atg8 lipidation. In selective autophagy these reactions could potentially be coupled to the cargo via the Atg19-Atg11-Atg9 interactions. We thus propose that Atg9 vesicles form seeds that establish membrane contact sites to initiate lipid transfer from compartments such as the endoplasmic reticulum.

Autophagy mediates the degradation of cytoplasmic material (the cargo) within lysosomes and ensures cellular homeostasis (1). Defects in autophagy have been associated with severe pathologies such as neurodegeneration, cancer, and infections (2). Cargo degradation is achieved by its sequestration within double membrane vesicles termed autophagosomes. These form de novo in an inducible manner and first appear as small membrane structures called isolation membranes (or phagophores), which gradually enclose the cargo as they

[#]correspondence should be addressed to: justyna.sawa-makarska@univie.ac.at or sascha.martens@univie.ac.at.
[*]These authors contributed equally to this work

Authors contributions
S.M., J.S.-M., and G.H. designed and supervised research, V.B., N.C., S.v.B., and V.N. designed research, J.S.-M., V.B., N.C., S.v.B., V.N, C.A., and M.S. performed research. All authors analyzed data and commented on the manuscript. S.M. and J.S.-M. wrote the manuscript.

Competing interests
S.M. is a member of the scientific advisory board of Casma Therapeutics.

Europe PMC Funders Author Manuscripts

grow. The assembly and growth of the isolation membranes is dependent on a number of conserved autophagy-related (Atg) proteins that act together in a hierarchical manner to nucleate and expand the isolation membranes (3–5). These include the Atg1 protein kinase complex (names refer to the yeast proteins), vesicles containing the Atg9 protein, the class III phosphatidylinositol 3-phosphate kinase complex 1 (PI3KC3-C1) producing the signaling lipid phosphatidylinositol 3-phosphate (PI3P), the PI3P-binding PROPPIN proteins, the lipid transfer protein Atg2 and the ubiquitin-like Atg12 and Atg8 conjugation systems (Figure 1A). During selective autophagy the interaction of cargo receptors with scaffold proteins directs this machinery towards specific cargos (6, 7). The attachment of Atg8 to the membrane lipid phosphatidylethanolamine (PE), referred to as lipidation, is the most downstream event of this cascade. How the biochemical activities of the autophagy machinery are orchestrated to mediate the formation of autophagosomes is not well understood. Especially enigmatic is the role of Golgi-derived Atg9 vesicles that are required for nucleation of the isolation membrane but do not provide the bulk of the autophagosomal membrane (8–11). Instead, the bulk of the lipids appears to be derived from other donor compartments and in particular the endoplasmic reticulum (ER) (12–19).

It has become clear that membrane contact sites are major mediators of non-vesicular lipid flow between compartments within the cell (20, 21). The flow of lipids is mediated by lipid transfer proteins that extract lipids from a donor membrane and transport them to an acceptor membrane. To elucidate how the various activities of the autophagy machinery act together during the nucleation of isolation membranes we reconstituted a large part of the yeast autophagy machinery in vitro.

Membrane recruitment of Atg12–Atg5-Atg16 by Atg21 and Atg2-Atg18

A hallmark of isolation membranes and completed autophagosomes is the conjugation of the ubiquitin-like Atg8 proteins to the headgroup of the lipid PE (22, 23). The Atg8 proteins are required for isolation membrane expansion, closure and cargo selectivity (24). The conjugation of Atg8 to PE is mediated by the E1-like Atg7 and the E2-like Atg3 proteins (22) as well as the Atg12–Atg5-Atg16 complex that acts in an E3-like manner (25) by activating and localizing Atg8-loaded Atg3 to the membrane (26, 27). Thus, the localization of the Atg12–Atg5-Atg16 complex is a crucial determinant of the site of Atg8 lipidation (28). Atg16 binds to the PI3P binding PROPPIN protein Atg21 (29). We asked if this interaction could mediate the recruitment of the Atg12–Atg5-Atg16 complex to PI3P-containing membranes, such as the isolation membrane. Indeed, Atg21 bound to PI3P containing giant unilamellar vesicles (GUVs) (Figure 1B). The Atg12–Atg5-Atg16 complex did not directly bind to this lipid composition, as expected (27) and was recruited only in the presence of Atg21 (Figure 1B). In cells the PI3P at the pre-autophagosomal structure (PAS) recruits another PROPPIN, the Atg18 protein in complex with the membrane tethering and lipid transfer protein Atg2 (16, 30–33). We asked if the Atg2-Atg18 complex could also interact with Atg12–Atg5-Atg16 and thereby contribute to its recruitment to PI3P positive membranes. Indeed, we detected a direct interaction between the two protein complexes in a pull-down assay (Figure 1C). We also observed that the presence of Atg2-Atg18 tended to accelerate the recruitment of the Atg12–Atg5-Atg16 complex to PI3P containing GUVs (Figure S1A). When tested by microscopy-based pull-down and membrane recruitment

experiments we observed that, as expected, Atg21 bound to the Atg12–Atg5-Atg16 complex via Atg16 (Figure S1B-C) (29) while the interaction of Atg2 was mediated by Atg5 and the interaction of Atg18 required the presence of Atg12 (Figure 1D-F and Figure S1D).

These results suggested the formation of a holocomplex on the membrane containing Atg21, Atg12–Atg5-Atg16 and Atg2-Atg18. We therefore dissected the recruitment of the individual components in more detail. Atg21 was the main driving force for the recruitment of Atg12–Atg5-Atg16 under the conditions tested (Figure 1G). In cells both PROPPINS, Atg18 and Atg21, as well as Atg2 contributed to the localization of Atg12–Atg5-Atg16 to the pre-autophagosomal structure (PAS) (Figure S2) (29). The residual recruitment of Atg12–Atg5-Atg16 in the triple deficient cells could be mediated by the Atg1 complex (34). In addition, deletion of Atg2, Atg18 and Atg21 strongly reduced Atg8 lipidation (Figure S3A) and deletion of any of the three proteins stalled the progression of the autophagic pathway (Figure S3B-C) (29, 30).

At the PAS the PI3KC3-C1 (consisting of the Vps34, Vps15, Atg6 and Atg14 subunits) phosphorylates phosphatidylinositol (PI) to PI3P (35). To address if the recruitment of the Atg12–Atg5-Atg16 complex and Atg8 lipidation could be driven by the activity of the PI3KC3-C1 through the PI3P-dependent recruitment of Atg2-Atg18 and Atg21, we added the purified PI3KC3-C1 to PI-containing GUVs in the presence of Atg21 and Atg2-Atg18 (Figure 2A). The Atg12–Atg5-Atg16 complex was recruited to the GUV membrane and this recruitment was dependent on the activity of the PI3KC3-C1 (Figure 2A and S4A). Atg21 alone was sufficient to recruit the Atg12–Atg5-Atg16 complex and to induce Atg8 lipidation on the GUVs (Figure 2B). These effects were enhanced when Atg2-Atg18 was also present (Figure 2B). We interpreted the localization of GFP-Atg8 on the membrane as lipidation because it was abolished when using a non-conjugatable form of Atg8 (GFP-Atg8-6xHis) and it strictly depended on the presence of the conjugation machinery Atg7 and Atg3 (Figure S4B).

Reconstitution of Atg8 lipidation on Atg9 proteoliposomes (PLs)

Autophagosome nucleation depends on the presence of Atg9 vesicles (8–11). In *S. cerevisiae* a few of these vesicles translocate to the autophagosome formation site (8). Because Atg9 is required for the recruitment of the PI3KC3-C1 to the site of autophagosome formation (36), we asked if the Atg9 vesicles could serve as platforms for the assembly of the autophagy machinery and thereby nucleate autophagosome formation. To this end, we reconstituted the purified Atg9 protein into small unilamellar vesicles (SUVs) to form proteoliposomes (PLs) (Figure S5A-D). In order to mimic the natural lipid composition of these vesicles, we isolated Atg9 vesicles from *S. cerevisiae* and determined their lipid composition by lipidomics (Figure S6A). The vesicles had a high PI content (44 %) (Figure S6B) (37), suggesting that they should be particularly good substrates for the PI3KC3-C1 complex. To test this, we tethered PLs containing Atg9-EGFP to GFP-Trap beads in order to image the recruitment of other factors by microscopy. The membrane of the PLs was labeled by incorporation of a blue membrane dye (ATTO390-DOPE). Upon incubation of the vesicles with the PI3KC3-C1, Atg21 and Atg2-Atg18 as well as the Atg12–Atg5-Atg16 complex, we observed recruitment of Atg12–Atg5-Atg16 to the Atg9 PLs (Figure 2C).

Consistent with the results above (Figure 1G, 2B), the recruitment was strongest in the presence of both Atg2-Atg18 and Atg21 (Figure 2D). We then asked if Atg8 could be conjugated to the Atg9 PLs in a manner that depends on PI3KC3-C1, Atg21, Atg2-Atg18 and Atg12–Atg5-Atg16. We therefore added Atg7 and Atg3 to the reaction, which now contained 14 polypeptides. We observed efficient Atg8 lipidation to the Atg9 PLs (Figure 2E). Reduction of the Atg8 signal upon addition of the wild type delipidating enzyme Atg4 but not its catalytic mutant (Figure S7A) showed that the detected mCherry-Atg8 signal at the beads was indeed due to lipidation.

Analogous to the results we observed regarding the Atg12–Atg5-Atg16 recruitment, Atg8 conjugation was relatively independent of the Atg2-Atg18 complex and was also weakly detectable in the absence of the PI3KC3-C1 (Figure 2F and S7B, C), likely because Atg21 shows residual binding to PI containing membranes. These results suggested a division of labor between Atg21 and Atg2-Atg18, where Atg21 plays a major role in the initial recruitment of Atg12–Atg5-Atg16 and the main function of Atg2-Atg18 could be membrane tethering and lipid transfer (16, 30–33).

Reconstitution of autophagosome nucleation in selective autophagy

In selective autophagy autophagosome nucleation must be coupled to the presence of cargo material (7). The cargo is recognized by cargo receptors such as p62 in human cells and Atg19 in *S. cerevisiae*. These cargo receptors link the autophagy machinery to the cargo via the FIP200/Atg11 proteins (6). Atg11 was shown to interact with Atg9 (38, 39). We purified full length Atg11 and, in agreement with (40), but in contrast to (39), we found Atg11 to be a constitutive dimer (Figure S8B). Atg11 bound directly to the N-terminus of Atg9 (Figure S8C). Next, we asked if the Atg19 cargo receptor could recruit the autophagy machinery including Atg9 vesicles to the cargo and subsequently initiate Atg8 conjugation. The cargo was mimicked by attachment of the GST-prApe1 propeptide (residues 1-41) to glutathione beads. These were incubated with the Atg19 cargo receptor and subsequently with Atg11. Atg11 was recruited to the beads in an Atg19 dependent manner. The recruitment was enhanced when a phospho-mimicking mutant of Atg19 (S390D, S391D, S396D) (41) was used (Figure S8A). Atg9 PLs and Atg9 vesicles isolated from cells (Figure S9) bound to the cargo beads in an Atg11 dependent manner (Figure 3A, B, Figure S8D). When we added the PI3KC3-C1, Atg2-Atg18, Atg21, Atg12–Atg5-Atg16, Atg3, Atg7 and Atg8 to the Atg9 PLs bound to the cargo beads, a reaction now containing almost the entire autophagy machinery, Atg8 was efficiently lipidated and anchored to the Atg9 PLs (Figure 3C). Isolated Atg9 vesicles could also serve as substrates for the lipidation reaction (Figure 3D), although the lipidation was markedly less prominent on the vesicles compared to the reconstituted PLs (Figure S10A). The Atg8 signal on the Atg9 vesicles was due to lipidation because it depended on the Atg12–Atg5-Atg16 complex (Figure 3D) and decreased upon addition of Atg4 (Figure 3E). Thus, the autophagy machinery can be redirected towards the cargo via the cargo receptor (Atg19) – scaffold (Atg11) – Atg9 axis (Figure 3, S10B). The Atg1-Atg13 complex was also recruited to these beads (Figure S10C). Thus, Atg11 and Atg9 vesicles are sufficient to recruit (almost) the entire autophagy machinery to the cargo.

Europe PMC Funders Author Manuscripts

Atg9 vesicles as acceptors for lipid transfer by Atg2

Owing to their small size Atg9 vesicles provide only limited surface for Atg8 lipidation and isolation membrane expansion. Furthermore, in addition to Atg9 they contain other proteins, which further reduce the effective surface for lipidation. This is consistent with our finding that Atg9 vesicles were less efficient substrates for Atg8 lipidation than Atg9 PLs (Figure 3, S10A). In order to estimate the available membrane surface of these vesicles we built a three-dimensional model of an Atg9 vesicle (Figure 4A, Movie S1). We based this model on an average diameter of 60 nm (Figure S9) (8), our proteomics data (Figure S6C, Data S1) and an average number of 28 Atg9 molecules per vesicle (8). In addition, we placed one molecule each of: PI3KC3-C1, Atg2-Atg18, Atg21, Atg12–Atg5-Atg16, and Atg3 loaded with Atg8 on the vesicular membrane (see Materials and Methods for details). With 70 proteins present in the modeled Atg9 vesicle, the accessibility of the membrane would be very limited. We calculated an effective dynamic surface coverage of 82% of the membrane area. Given that peripheral membrane proteins may have been lost during the isolation, the very stringent selection of proteins from mass spectrometric data used for modeling, and the fact that we assumed the Atg9 N- and C-termini not to interact with the vesicular membrane, the actual free surface may be even lower and difficult to reach for incoming proteins. Thus, Atg9 vesicles may require lipid influx in order to transform into an efficient substrate for Atg8 lipidation.

The lipid transfer protein Atg2 is recruited to the Atg9 vesicles (Figure 4B) and tethers Atg9 to the ER in cells (16). The interaction between ATG2A and ATG9A is important for isolation membrane expansion in mammalian cells (42). Atg2-mediated lipid transfer from the ER into the membrane of the Atg9 vesicle may therefore enable Atg8 lipidation and subsequent expansion of the spherical Atg9 vesicles, converting them into the disk-shaped isolation membranes.

To test if Atg2 could transport lipids for Atg8 conjugation, we mixed two populations of liposomes. One population (SUV A) contained a lipid composition that efficiently recruited the lipidation machinery (27) but did not contain PE as substrate for Atg8 conjugation. The other population (SUV B) contained PE but was not efficiently targeted by the lipidation machinery (Figure 4C, Figure S11C). Upon addition of Atg2-Atg18, which is active in lipid transport (Figure S11A-B) we detected a significantly increased lipidation of Atg8 demonstrating that Atg2-Atg18 could directly enhance Atg8 lipidation (Figure 4C). Because phosphatidylserine (PS) can also serve as substrate for Atg8 lipidation in vitro (43), the actual stimulatory effect of Atg2-Atg18 on Atg8 lipidation may be even higher. To exclude the possibility that Atg2-Atg18 by direct binding allosterically activated the E3, we conjugated Atg8 to PE-containing SUVs in the presence or absence of Atg2-Atg18 and we could not observe significant differences in Atg8 lipidation (Figure S11D). Atg9 PLs also served as acceptors for Atg2-mediated lipid transport (Figure 4D). We therefore asked if the lipids transported into Atg9 PLs could serve as substrates for Atg8 lipidation. Atg9 PLs lacking PE and PS were mixed with a second population of liposomes containing these lipids. We then added the Atg2-Atg18 in the presence of the PI3KC3-C1, Atg21, Atg12–Atg5-Atg16, Atg7, Atg3 and Atg8 (Figure 4E). Indeed, we found Atg8 lipidation, as monitored by immunoblotting, was accelerated in the presence of Atg2-Atg18 (Figure 4E).

To confirm that Atg8 lipidation occurred on the Atg9 PLs, we pulled down the Atg9 PLs using GFP-Trap beads and found lipidated Atg8 only in the presence of Atg2-Atg18 (Figure 4E, arrow).

Discussion

Here we present a near full in vitro reconstitution of the events occurring during autophagosome nucleation in selective autophagy. Particularly, we could show that Atg9 vesicles are substrates of PI3KC3-C1 and that the PI3P generated in situ mediates the successive recruitment of Atg21, Atg2-Atg18 and the Atg12–Atg5-Atg16 complex as prerequisites for the subsequent Atg8 lipidation.

The role of Atg9 vesicles has remained mysterious. On the one hand, they are required for early steps of autophagosome formation but, on the other hand, they comprise only a minor fraction of lipids required to form the autophagosomal membrane (8–11). Autophagosomes are generated in proximity to the endoplasmic reticulum (ER) but their membranes are clearly distinct from the ER membrane (13–19). Our results show that Atg9 vesicles form a platform for the recruitment of the autophagy machinery. Among them is the membrane tethering and lipid transfer protein Atg2 (16, 30–33), which can transfer lipids at a rate enabling it to be a major contributor to isolation membrane expansion (44). It has become clear that lipid transfer at membrane contact sites provides the communication and membrane flow between intracellular compartments. However, lipid transfer can only occur between existing donor and acceptor compartments. Atg9 vesicles may thus form seeds for the initial establishment of membrane contact sites. Therefore, quantitative Atg8 lipidation may only occur upon lipid influx from the ER into the Atg9 vesicle, gradually converting it into the disk-shaped isolation membrane (Figure 5). In this manner, Atg9 vesicles could seed a biochemically unique membrane, the isolation membrane, largely devoid of transmembrane proteins (45, 46). To ensure the expansion of the isolation membrane the incoming lipids must be distributed to its inner leaflet, an action that would require flippase or scramblase activity. Interestingly, we found two flippases (Drs2 and Neo1) present in our Atg9 vesicle proteomics analysis. Multiple individual nucleation events followed by ESCRT-mediated membrane sealing may be required for the formation of larger autophagosomes (47–49).

In addition, the Golgi-derived Atg9 vesicles isolated from cells might be tightly packed with proteins. The influx of loosely packed lipids from the ER might thus render them good substrates for subsequent Atg8 lipidation apart from the expansion of the free membrane area. In fact, autophagosomal membranes contain a high proportion of lipids with unsaturated fatty acids (12). Apart from serving as acceptors for lipid influx, Atg9 vesicles may also kickstart local lipid synthesis (12). Consistently, we found Faa1 and Faa4 in our Atg9 vesicle proteomics.

During selective autophagy, cargo material is specifically sequestered by autophagosomes. It has become clear that cargo receptors act upstream of the autophagy machinery by recruiting scaffold proteins to the cargo (50–56). Here we fully reconstitute the cargo receptor and scaffold dependent recruitment of the autophagy machinery to the cargo material and

demonstrate that this system is sufficient to promote local Atg8 lipidation. Future work will reveal how the recruitment of the autophagy machinery including the Atg9 vesicles is sterically and temporally coupled to the formation of membrane contact sites with the ER.

Materials and Methods Summary

The full version of the Material and methods is available as supplementary material.

Protein expression and purification

Atg19 (1-374 residues), the Atg19-3D and Atg19-3DΔLIR mutants were expressed and purified as described elsewhere (57, 58). mEGFP/mCherry-Atg8-ΔR117 was expressed and purified as described in (27).

6xHis-TEV-Atg21, 6xHis-TEV-mEGFP-Atg21, 6xHis-TEV-mCherry-Atg21, 6xHis-Atg18-mEGFP and Atg9-NTD(1-285)-mEGFP were all expressed in *E. coli*. Rosetta pLysS.

Atg2-Atg18-CBP, Atg2-GFP-Atg18-CBP and Atg2-mCherry-Atg18-CBP were purified from the SMY373, SMY374 and SMY439 yeast strains, respectively.

6xHis-TEV-Atg2-mEGFP, PI3KC3-C1, protA-TEV-Atg1-Atg13, 6xHis-TEV-mEGFP/mCherry-Atg11 and 6xHis-TEV-Atg9-mEGFP/mCherry were all expressed in the baculovirus expression system.

All soluble proteins were purified via affinity chromatography followed by size exclusion chromatography.

For full length Atg9-mEGFP/mCherry, cell membranes were collected by centrifuging the cleared cell lysate at 40 000 rpm for 1 h. The membranes were resuspended for 2 h at 4°C in lysis buffer containing 2 % DDM. After 2 h of incubation the insoluble material was removed by centrifugation at 40 000 rpm for 1 h. Atg9 was then purified by affinity chromatography followed by size exclusion chromatography in the presence of 0,2 % DDM. In order to concentrate the protein without increasing the detergent concentration, the fractions containing protein were incubated with 150 µl of NiNTA beads for 3 h at 4°C. The beads were washed several times with 25 mM Tris pH 7.4, 300 mM NaCl, 0.04 % DDM. The protein was eluted in the desired volume of buffer supplemented with 300 mM imidazole. A final dialysis was performed overnight at 4°C against 25 mM Tris pH 7.4, 300 mM NaCl, 0.04 % DDM.

Atg9 PLs formation and analysis

Small unilamellar vesicles (SUVs, liposomes) destined for the reconstitution of Atg9 PLs were prepared with a lipid composition mimicking the lipid composition of the endogenous Atg9 vesicles determined in this study (for details see Table 2). For the incorporation of Atg9, the SUVs were treated with CHAPS (Avanti Polar Lipids, Inc.). The SUV suspension was brought up to 2.5 % CHAPS and incubated at RT for 1 h. The SUV suspension was then mixed 1 to 1 with a 1 µM Atg9 solution in 0.04 % DDM. The mixture was incubated at RT for another 90 min and then diluted by a factor of 10 in Tris 25 mM Tris pH 7.4, 300 mM

Europe PMC Funders Author Manuscripts

NaCl in order to reach a detergent concentration below the CMC of both detergents. The resulting PLs solution was dialyzed overnight at 4°C against 25 mM Tris pH 7.4, 300 mM NaCl supplemented with 0.1 g of BioBeads SM2 (BioRad) per liter of buffer. Finally, BioBeads were added directly to the sample and incubated 1 hour at RT. The insoluble material that did not get incorporated into liposomes was removed by centrifuging 30 min at 18000 rpm. The supernatant containing Atg9 PLs was collected and used for subsequent experiments.

Membrane recruitment - GUV assays

To image Atg21, Atg2-Atg18 and Atg12–Atg5-Atg16 membrane recruitment 15 μl of the electroformed GUVs were transferred to a 96-well glass-bottom microplate (Greiner Bio-One) and the respective proteins were added to the final concentration of 1 μM in a final reaction volume of 30 μl in a reaction buffer 25 mM HEPES at pH 7.5, 150 mM NaCl. In every experiment including GUVs, before the GUVs and the proteins were pipetted onto the plate, the wells were blocked with a blocking solution (2.5 mg/ml BSA in 50 mM TrisHCl pH 7.4, 150mM NaCl) for 1 h and washed twice with the reaction buffer.

For Atg21, Atg2-Atg18 and Atg12–Atg5-Atg16 membrane recruitment in the presence of PI3KC3-C1 experiments mixes containing respective proteins, 0.1 mM ATP or 0.1 mM AMP-PNP, 0.5 mM $MgCl_2$, 2 mM $MnCl_2$ and 1 mM EGTA in a final volume of 15 μl were prepared. The final concentration of proteins in the reaction mixes were: 50 nM for PI3KC3-C1, 400 nM for Atg21, 400 nM for Atg2-GFP-Atg18 and 40 nM for Atg12–Atg5-Atg16-mCherry. The reaction mixes were added to the well already containing 15 μl of the electroformed GUVs. For the time course experiment, the imaging started 5 min after the addition of the reaction mix to GUVs. The images were acquired for 45 min at the indicated time points of reaction.

In vitro reconstitution of Atg8 lipidation on GUVs

To image the PI3KC3-C1-dependent Atg8–PE conjugation to GUVs, mixes containing respective proteins (according to the experimental setup), 0.5 mM ATP, 0.5 mM $MgCl_2$, 2 mM $MnCl_2$ and 1 mM EGTA in a final volume of 15 μl were prepared. The reaction buffer contained 25 mM HEPES at pH 7.5, 150 mM NaCl. The final concentrations of proteins in the reaction mixes were: 50 nM for PI3KC3-C1, 400 nM for Atg21, 400 nM for Atg2-Atg18, 40 nM for Atg12–Atg5-Atg16-mCherry, 80 nM for Atg7, 80 nM for Atg3, 400 nM GFP-Atg8ΔR117 and 400 nM GFP-Atg8-6xHis. The reaction mixes were added to wells of a 96-well glass-bottom microplate (Greiner Bio-One) already containing 15 μl of the electroformed GUVs. Concentrations of proteins and cofactors used were calculated for the final 30 μl volume of the experiment.

Microscopy-based protein-protein interaction assay

For the experiments shown in Figures 2B and 2G giant unilamellar vesicles (GUVs) were prepared. Preparation was carried out as described above. Assays were performed under

equilibrium conditions and mEGFP-Atg21, 6xHis-Atg21, Atg12–Atg5-Atg16-mCherry and Atg2-GFP-Atg18-CBP were added at a final concentration of 500 nM.

For Figure 1 D-F Atg12–Atg5-Atg16-mCherry, Atg5-mCherry-Atg16(1-46) and Atg16-mCherry were recruited to RFP-TRAP beads (Chromotek). Assays were performed under equilibrium conditions with 2 μM of the prey proteins Atg2-GFP-Atg18-CBP, Atg2-mEGFP and Atg18-mEGFP.

Isolation of endogenous Atg9 vesicles

To isolate endogenous Atg9 vesicles, we cloned versions of Atg9 tagged with a fluorophore (mEGFP or mCherry) and a TEV cleavable affinity tag (9xmyc or TAP). These constructs were used to replace the endogenous *ATG9* gene in haploid BY474x *S. cerevisiae* cells, putting the expression under the control of the endogenous *ATG9* promoter. Constructs were then integrated into wild type or *pep4*Δ strains.

Strains were grown, harvested and lysed. Cleared cell lysate was incubated with the appropriate affinity beads (coated with either IgG or anti-myc antibody) at 4°C for 1 h. The beads were then washed, the vesicles were released by TEV cleavage at 4°C for an hour and the supernatant was collected.

In vitro reconstitution of Atg8 lipidation on Atg9 PL or Atg9 vesicles bound to cargomimetic beads

Assembly of the cargo-mimetic beads

Glutathione sepharose 4B beads (GE Healthcare) were first equilibrated in 25 mM Tris pH 7.4, 300 mM NaCl. Beads were mixed with the same volume of a 30 μM solution of GST-prApe1 (1-41), 30 μM solution of Atg19-3DΔLIR mutant and 30 μM of Atg11. The mixture was incubated for 1 h at 4°C and the beads were subsequently washed 3 times.

Recruitment of Atg9 PLs or Atg9 vesicles to the cargo-mimetic beads

10 μl of cargo-mimetic beads were mixed with either 200 μl of Atg9-mCherry PLs solution or an equal volume of TEV-eluted Atg9-EGFP-vesicles. The mixture was incubated 2h at 4°C and the beads were subsequently washed once

In vitro Atg8 lipidation

0.5 μl of cargo-mimetic beads coated with Atg9-mCherry PL or Atg9-EGFP vesicles were pipetted into the wells of a 384-well glass-bottom microplate (Greiner Bio-One) containing 0.5 mM ATP, 0.5 mM $MgCl_2$, 2 mM $MnCl_2$ and 1 mM EGTA in a final volume of 15 μl. The final concentrations of proteins in the reaction mixes were: 50 nM for PI3KC3-C1, 400 nM for Atg21, 400 nM for Atg2-Atg18, 40 nM for Atg12–Atg5-Atg16, 100 nM for Atg7, 100 nM for Atg3 and 400 nM for EGFP-Atg8ΔR117 (200 nM of mCherry-Atg8ΔR117 for Atg9 vesicles). The reactions were incubated for 2h at room temperature in the dark and the beads were imaged using confocal microscope LSM700 (Zeiss) with 20x objective and processed with ImageJ software.

To de-conjugate Atg8 from Atg9 vesicles Atg4 or Atg4C147S was added at a final concentration of 0.5 μM together with EDTA at a final concentration of 2 mM and microscopy images were taken at the indicated time points.

Supplementary Material

Refer to Web version on PubMed Central for supplementary material.

Acknowledgments

We thank Graham Warren for comments on the manuscript. We thank Dr. Susanne Brodesser and the CECAD Lipidomics/Metabolomics Facility for performing lipidomics analyses. We thank Markus Hartl from the Max Perutz Labs Mass Spectrometry Facility, the Max Perutz Labs BioOptics Facility, and the VBCF Electron Microscopy Facility for technical support and the VBCF for providing the MS instrument pool. Anti-CBP antibody and yeast strains carrying Atg2-Atg18 expression cassettes were kindly provided by Prof. Dr. Christian Ungermann. We thank Lisa Pietrek for help with the simulation setup and Dorotea Fracchiolla for expressing and purifying unlabeled Atg21.

Funding

This work was supported by the ERC grant No.646653 (S.M.), by the Austrian Science Fund FWF, No. P32814-B (S.M.) and T724-B20 (J.S.-M.), Human Frontier Science Program RGP0026/2017 (S.M., G.H. and S.v.B.), an OEAW Doc fellowship (C.A.), and the Max Planck Society (G.H., S.v.B., M.G.).

Data availability

All data are available in the manuscript or the supplementary material.

References

1. Mizushima N, Komatsu M. Autophagy: renovation of cells and tissues. Cell. 2011; 147:728–741. [PubMed: 22078875]
2. Levine B, Kroemer G. Biological Functions of Autophagy Genes: A Disease Perspective. Cell. 2019; 176:11–42. [PubMed: 30633901]
3. Xie Z, Klionsky DJ. Autophagosome formation: core machinery and adaptations. Nature Cell Biology. 2007; 9:1102. [PubMed: 17909521]
4. Mizushima N, Yoshimori T, Ohsumi Y. The Role of Atg Proteins in Autophagosome Formation. Annual Review of Cell and Developmental Biology. 2011; 27:107–132.
5. Lamb CA, Yoshimori T, Tooze SA. The autophagosome: origins unknown, biogenesis complex. Nature Reviews Molecular Cell Biology. 2013; 14:759. [PubMed: 24201109]
6. Turco E, Fracchiolla D, Martens S. Recruitment and Activation of the ULK1/Atg1 Kinase Complex in Selective Autophagy. Journal of Molecular Biology. 2019
7. Zaffagnini G, Martens S. Mechanisms of Selective Autophagy. Journal of Molecular Biology. 2016; 428:1714–1724. [PubMed: 26876603]
8. Yamamoto H, et al. Atg9 vesicles are an important membrane source during early steps of autophagosome formation. The Journal of Cell Biology. 2012; 198:219. [PubMed: 22826123]
9. Orsi A, et al. Dynamic and transient interactions of Atg9 with autophagosomes, but not membrane integration, are required for autophagy. Molecular Biology of the Cell. 2012; 23:1860–1873. [PubMed: 22456507]
10. Young ARJ, et al. Starvation and ULK1-dependent cycling of mammalian Atg9 between the TGN and endosomes. Journal of Cell Science. 2006; 119:3888. [PubMed: 16940348]
11. Ohashi Y, Munro S. Membrane Delivery to the Yeast Autophagosome from the Golgi–Endosomal System. Molecular Biology of the Cell. 2010; 21:3998–4008. [PubMed: 20861302]

Europe PMC Funders Author Manuscripts

12. Schütter M, Giavalisco P, Brodesser S, Graef M. Local Fatty Acid Channeling into Phospholipid Synthesis Drives Phagophore Expansion during Autophagy. Cell. 2020; 180:135–149. e114 [PubMed: 31883797]
13. Axe EL, et al. Autophagosome formation from membrane compartments enriched in phosphatidylinositol 3-phosphate and dynamically connected to the endoplasmic reticulum. The Journal of Cell Biology. 2008; 182:685. [PubMed: 18725538]
14. Graef M, Friedman JR, Graham C, Babu M, Nunnari J. ER exit sites are physical and functional core autophagosome biogenesis components. Molecular Biology of the Cell. 2013; 24:2918–2931. [PubMed: 23904270]
15. Hamasaki M, et al. Autophagosomes form at ER–mitochondria contact sites. Nature. 2013; 495:389. [PubMed: 23455425]
16. Gómez-Sánchez R, et al. Atg9 establishes Atg2-dependent contact sites between the endoplasmic reticulum and phagophores. The Journal of Cell Biology. 2018; 217:2743. [PubMed: 29848619]
17. Hayashi-Nishino M, et al. A subdomain of the endoplasmic reticulum forms a cradle for autophagosome formation. Nature Cell Biology. 2009; 11:1433. [PubMed: 19898463]
18. Ylä-Anttila P, Vihinen H, Jokitalo E, Eskelinen E-L. 3D tomography reveals connections between the phagophore and endoplasmic reticulum. Autophagy. 2009; 5:1180–1185. [PubMed: 19855179]
19. Nishimura T, et al. Autophagosome formation is initiated at phosphatidylinositol synthase-enriched ER subdomains. The EMBO Journal. 2017; 36:1719–1735. [PubMed: 28495679]
20. Wu H, Carvalho P, Voeltz GK. Here, there, and everywhere: The importance of ER membrane contact sites. Science. 2018; 361 eaan5835 [PubMed: 30072511]
21. Cohen S, Valm AM, Lippincott-Schwartz J. Interacting organelles. Current Opinion in Cell Biology. 2018; 53:84–91. [PubMed: 30006038]
22. Ichimura Y, et al. A ubiquitin-like system mediates protein lipidation. Nature. 2000; 408:488. [PubMed: 11100732]
23. Kabeya Y, et al. LC3, a mammalian homologue of yeast Apg8p, is localized in autophagosome membranes after processing. The EMBO Journal. 2000; 19:5720–5728. [PubMed: 11060023]
24. Slobodkin MR, Elazar Z. The Atg8 family: multifunctional ubiquitin-like key regulators of autophagy. Essays In Biochemistry. 2013; 55:51. [PubMed: 24070471]
25. Hanada T, et al. The Atg12-Atg5 Conjugate Has a Novel E3-like Activity for Protein Lipidation in Autophagy. Journal of Biological Chemistry. 2007; 282:37298–37302.
26. Zheng Y, et al. A switch element in the autophagy E2 Atg3 mediates allosteric regulation across the lipidation cascade. Nature Communications. 2019; 10:3600.
27. Romanov J, et al. Mechanism and functions of membrane binding by the Atg5-Atg12/Atg16 complex during autophagosome formation. EMBO J. 2012; 31:4304–4317. [PubMed: 23064152]
28. Fujita N, et al. The Atg16L Complex Specifies the Site of LC3 Lipidation for Membrane Biogenesis in Autophagy. Molecular Biology of the Cell. 2008; 19:2092–2100. [PubMed: 18321988]
29. Juris L, et al. PI3P binding by Atg21 organises Atg8 lipidation. The EMBO Journal. 2015; 34:955. [PubMed: 25691244]
30. Obara K, Sekito T, Niimi K, Ohsumi Y. The Atg18-Atg2 Complex Is Recruited to Autophagic Membranes via Phosphatidylinositol 3-Phosphate and Exerts an Essential Function. Journal of Biological Chemistry. 2008; 283:23972–23980.
31. Valverde DP, et al. ATG2 transports lipids to promote autophagosome biogenesis. The Journal of Cell Biology. 2019; 218:1787. [PubMed: 30952800]
32. Osawa T, et al. Atg2 mediates direct lipid transfer between membranes for autophagosome formation. Nature Structural & Molecular Biology. 2019; 26:281–288.
33. Kotani T, Kirisako H, Koizumi M, Ohsumi Y, Nakatogawa H. The Atg2-Atg18 complex tethers pre-autophagosomal membranes to the endoplasmic reticulum for autophagosome formation. Proceedings of the National Academy of Sciences. 2018; 115:10363.
34. Harada K, et al. Two distinct mechanisms target the autophagy-related E3 complex to the pre-autophagosomal structure. Elife. 2019; 8 e43088 [PubMed: 30810528]

35. Kihara A, Noda T, Ishihara N, Ohsumi Y. Two Distinct Vps34 Phosphatidylinositol 3– Kinase Complexes Function in Autophagy and Carboxypeptidase Y Sorting in Saccharomyces cerevisiae. The Journal of Cell Biology. 2001; 152:519. [PubMed: 11157979]
36. Suzuki SW, et al. Atg13 HORMA domain recruits Atg9 vesicles during autophagosome formation. Proceedings of the National Academy of Sciences. 2015; 112:3350.
37. van Meer G, Voelker DR, Feigenson GW. Membrane lipids: where they are and how they behave. Nature Reviews Molecular Cell Biology. 2008; 9:112. [PubMed: 18216768]
38. He C, et al. Recruitment of Atg9 to the preautophagosomal structure by Atg11 is essential for selective autophagy in budding yeast. The Journal of Cell Biology. 2006; 175:925. [PubMed: 17178909]
39. Matscheko N, Mayrhofer P, Rao Y, Beier V, Wollert T. Atg11 tethers Atg9 vesicles to initiate selective autophagy. PLOS Biology. 2019; 17 e3000377 [PubMed: 31356628]
40. Suzuki H, Noda NN. Biophysical characterization of Atg11, a scaffold protein essential for selective autophagy in yeast. FEBS Open Bio. 2018; 8:110–116.
41. Pfaffenwimmer T, et al. Hrr25 kinase promotes selective autophagy by phosphorylating the cargo receptor Atg19. EMBO Rep. 2014; 15:862–870. [PubMed: 24968893]
42. Tang Z, et al. TOM40 Targets Atg2 to Mitochondria-Associated ER Membranes for Phagophore Expansion. Cell Reports. 2019; 28:1744–1757. e1745 [PubMed: 31412244]
43. Oh-oka K, Nakatogawa H, Ohsumi Y. Physiological pH and Acidic Phospholipids Contribute to Substrate Specificity in Lipidation of Atg8. Journal of Biological Chemistry. 2008; 283:21847–21852.
44. von Bülow S, Hummer G. Kinetics of Atg2-mediated lipid transfer from the ER can account for phagophore expansion. bioRxiv. 2020 2020.2005.2012.090977
45. Baba M, Takeshige K, Baba N, Ohsumi Y. Ultrastructural analysis of the autophagic process in yeast: detection of autophagosomes and their characterization. J Cell Biol. 1994; 124:903–913. [PubMed: 8132712]
46. Fengsrud M, Erichsen ES, Berg TO, Raiborg C, Seglen PO. Ultrastructural characterization of the delimiting membranes of isolated autophagosomes and amphisomes by freeze-fracture electron microscopy. Eur J Cell Biol. 2000; 79:871–882. [PubMed: 11152279]
47. Takahashi Y, et al. An autophagy assay reveals the ESCRT-III component CHMP2A as a regulator of phagophore closure. Nature Communications. 2018; 9 2855
48. Zhen Y, et al. ESCRT-mediated phagophore sealing during mitophagy. Autophagy. 2019:1–16.
49. Zhou F, et al. Rab5-dependent autophagosome closure by ESCRT. Journal of Cell Biology. 2019; 218:1908–1927.
50. Ravenhill BJ, et al. The Cargo Receptor NDP52 Initiates Selective Autophagy by Recruiting the ULK Complex to Cytosol-Invading Bacteria. Molecular Cell. 2019
51. Smith MD, Wilkinson S. CCPG1, an unconventional cargo receptor for ER-phagy, maintains pancreatic acinar cell health. Molecular & cellular oncology. 2018; 5 e1441631 [PubMed: 30263939]
52. Vargas JNS, et al. Spatiotemporal Control of ULK1 Activation by NDP52 and TBK1 during Selective Autophagy. Molecular Cell. 2019
53. Turco E, et al. FIP200 Claw Domain Binding to p62 Promotes Autophagosome Formation at Ubiquitin Condensates. Mol Cell. 2019
54. Shintani T, Klionsky DJ. Cargo Proteins Facilitate the Formation of Transport Vesicles in the Cytoplasm to Vacuole Targeting Pathway. Journal of Biological Chemistry. 2004; 279:29889–29894.
55. Kamber, Roarke A; Shoemaker, Christopher J; Denic, V. Receptor-Bound Targets of Selective Autophagy Use a Scaffold Protein to Activate the Atg1 Kinase. Molecular Cell. 2015; 59:372–381. [PubMed: 26166702]
56. Torggler R, et al. Two Independent Pathways within Selective Autophagy Converge to Activate Atg1 Kinase at the Vacuole. Molecular Cell. 2016; 64:221–235. [PubMed: 27768871]
57. Fracchiolla D, et al. Mechanism of cargo-directed Atg8 conjugation during selective autophagy. Elife. 2016; 5 e18544 [PubMed: 27879200]

58. Sawa-Makarska J, et al. Cargo binding to Atg19 unmasks additional Atg8 binding sites to mediate membrane–cargo apposition during selective autophagy. Nat Cell Biol. 2014; 16:425–433. [PubMed: 24705553]

Europe PMC Funders Author Manuscripts

Europe PMC Funders Author Manuscripts

One sentence summary

Near complete reconstitution of the autophagy machinery defines Atg9 vesicles as nucleators of autophagosomes.

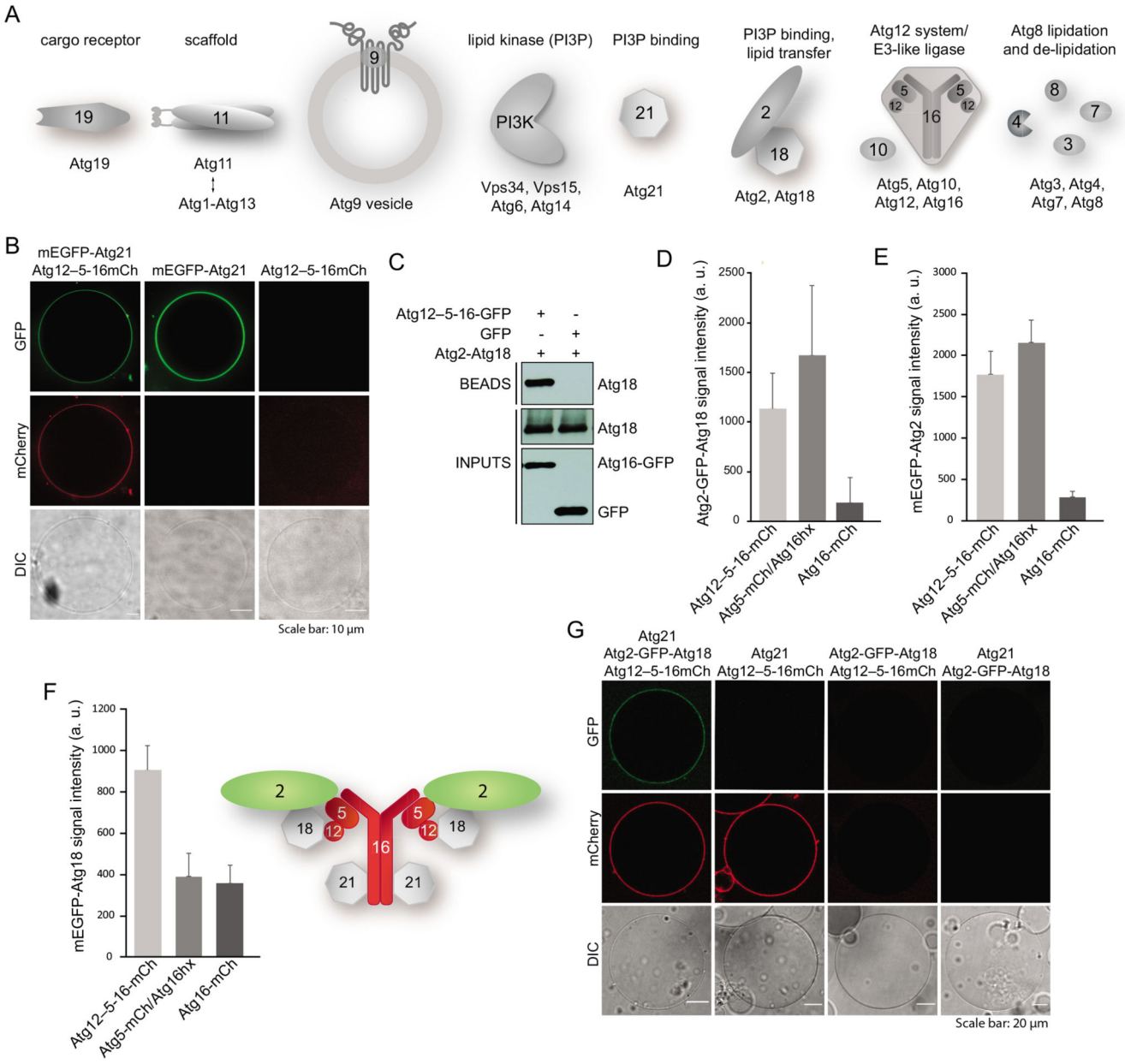

Figure 1. Membrane recruitment of the Atg12–Atg5-Atg16 complex by PROPPINs.

(**A**) Cartoon showing proteins used in this study. PI3KC3-C1 will be labelled as PI3K in schemes and figures. (**B**) GUVs containing PI3P (57% POPC, 25.5% POPS, 15% POPE, 2.5% PI3P) were incubated with 1 µM Atg12–Atg5-Atg16-mCherry supplemented with 1 µM eGFP-Atg21 or with only 1 µM eGFP-Atg21 or with only 1 µM Atg12–Atg5-Atg16-mCherry and imaged by microscopy (**C**) GFP-Trap pull down using Atg12–Atg5-Atg16-GFP or GFP as bait and Atg2-Atg18 as prey. The bait and the prey proteins were detected by immunoblotting with anti-GFP and anti-CBP antibodies respectively. (**D-F**) Quantification of the pulldown experiment mapping the interaction between Atg12–Atg5-Atg16 and Atg2-Atg18 shown in Figure S1D. The quantification is based on three independent experiments. Standard deviations are shown. A schematic representation of the putative holocomplex

Europe PMC Funders Author Manuscripts

composed of Atg12–Atg5-Atg16, Atg2-Atg18 and Atg21 is shown as a cartoon insert. (**G**) GUVs of the same lipid composition as in (B) were incubated with Atg12–Atg5-Atg16-mCherry, Atg21 or Atg2-GFP-Atg18 at 1 μM final concentration each and the recruitment of the proteins to the membrane was imaged by microscopy.

Europe PMC Funders Author Manuscripts

Europe PMC Funders Author Manuscripts

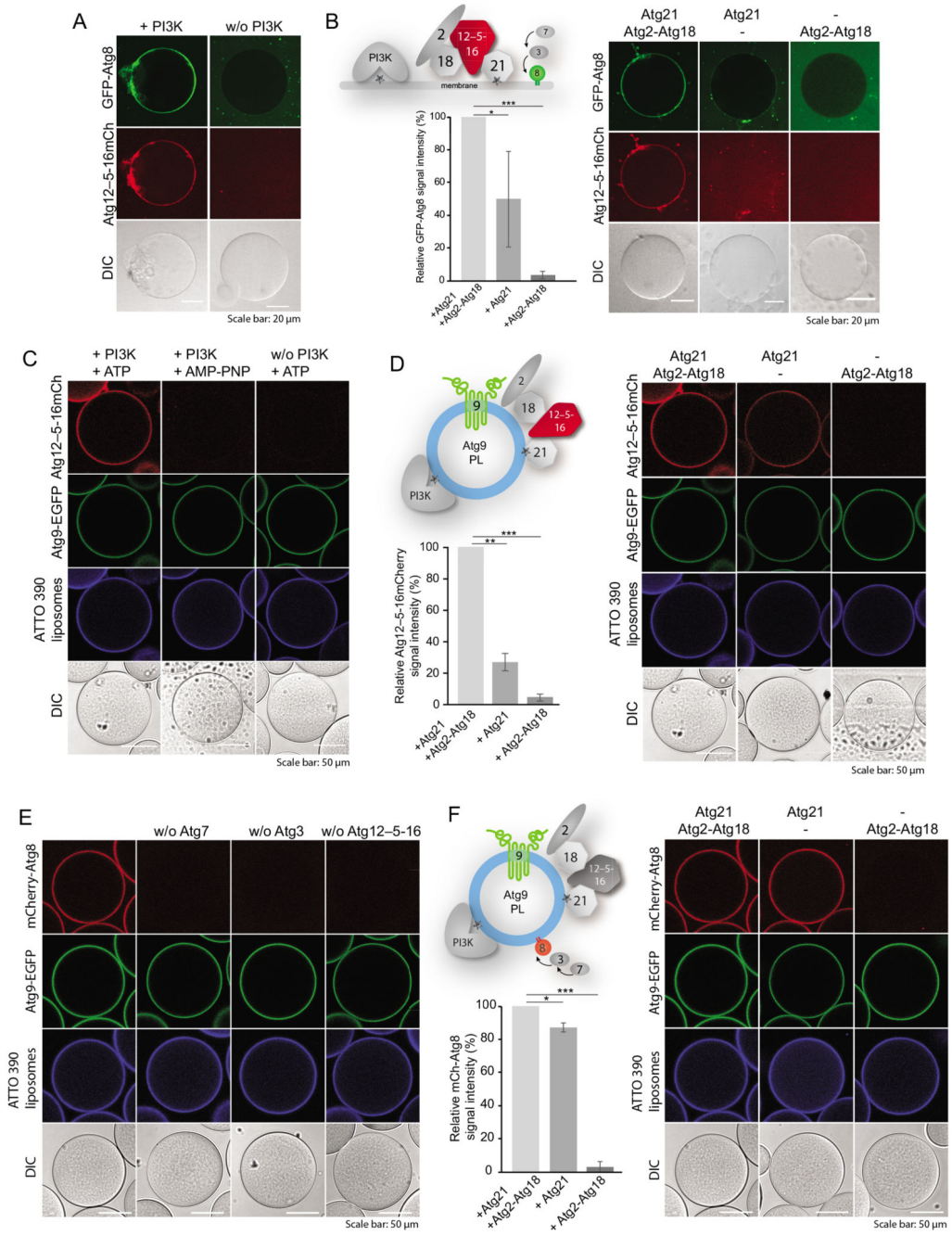

Figure 2. In vitro reconstitution of PI3KC3-C1-dependent Atg8 lipidation.

(**A**) The Atg8–PE conjugation machinery (Atg7, Atg3, Atg12–Atg5-Atg16-mCherry, GFP-Atg8ΔR117), PROPPINs (Atg21, Atg2-Atg18) were added to GUVs (55% DOPC, 10% DOPS, 17% DOPE, 18% liver PI) and incubated in the presence or absence of PI3KC3-C1 and cofactors (ATP, $MnCl_2$, $MgCl_2$, EGTA). Microscopy images of representative GUVs are shown. The proteins included in the experiment are depicted in the cartoon insert to the right. (**B**) Atg8 lipidation to GUVs depends on the presence of Atg21. GUVs as in (A) were incubated with Atg8–PE conjugation machinery proteins as in (A) and PI3KC3-C1 in the

presence of either one or both PROPPINs. The quantification of the GFP signal on GUVs from three independent experiments is shown to the left. (**C**) Atg12–Atg5-Atg16 recruitment to Atg9 PLs depends on the activity of PI3KC3-C1. GFP-Trap beads were coated with Atg9-EGFP PLs and incubated with Atg21, Atg2-Atg18 and Atg12–Atg5-Atg16-mCherry in the presence or absence of PI3KC3-C1 and ATP or in the presence of PI3KC3-C1 and AMP-PNP. Microscopy images of representative beads are shown. (**D**) Beads as in (C) were incubated with Atg12–Atg5-Atg16-mCherry and PI3KC3-C1 in the presence of either one or both PROPPINs. The quantification of mCherry signal on beads from three independent experiments is shown on the left. (**E**) Reconstitution of Atg8-lipidation to Atg9 PLs. Beads as in (C) were incubated with PI3KC3-C1, ATP, Atg21, Atg2-Atg18, mCherry-Atg8ΔR117, Atg7, Atg3, Atg12–Atg5-Atg16 each time omitting one of the Atg8–PE conjugation machinery proteins as indicated above the microscopy images of representative beads. (**F**) Atg8 lipidation to Atg9 PLs depends on the presence of Atg21. Beads as in (C) were incubated with PI3KC3-C1, ATP, mCherry-Atg8ΔR117, Atg7, Atg3, Atg12–Atg5-Atg16 in the presence of either one or both PROPPINs. The quantification of mCherry signal on the beads from three independent experiments is shown to the left. Significance is indicated using p-values from Student's t-test: * ($p \leq 0.05$), ** ($p \leq 0.01$) and *** ($p \leq 0.001$).

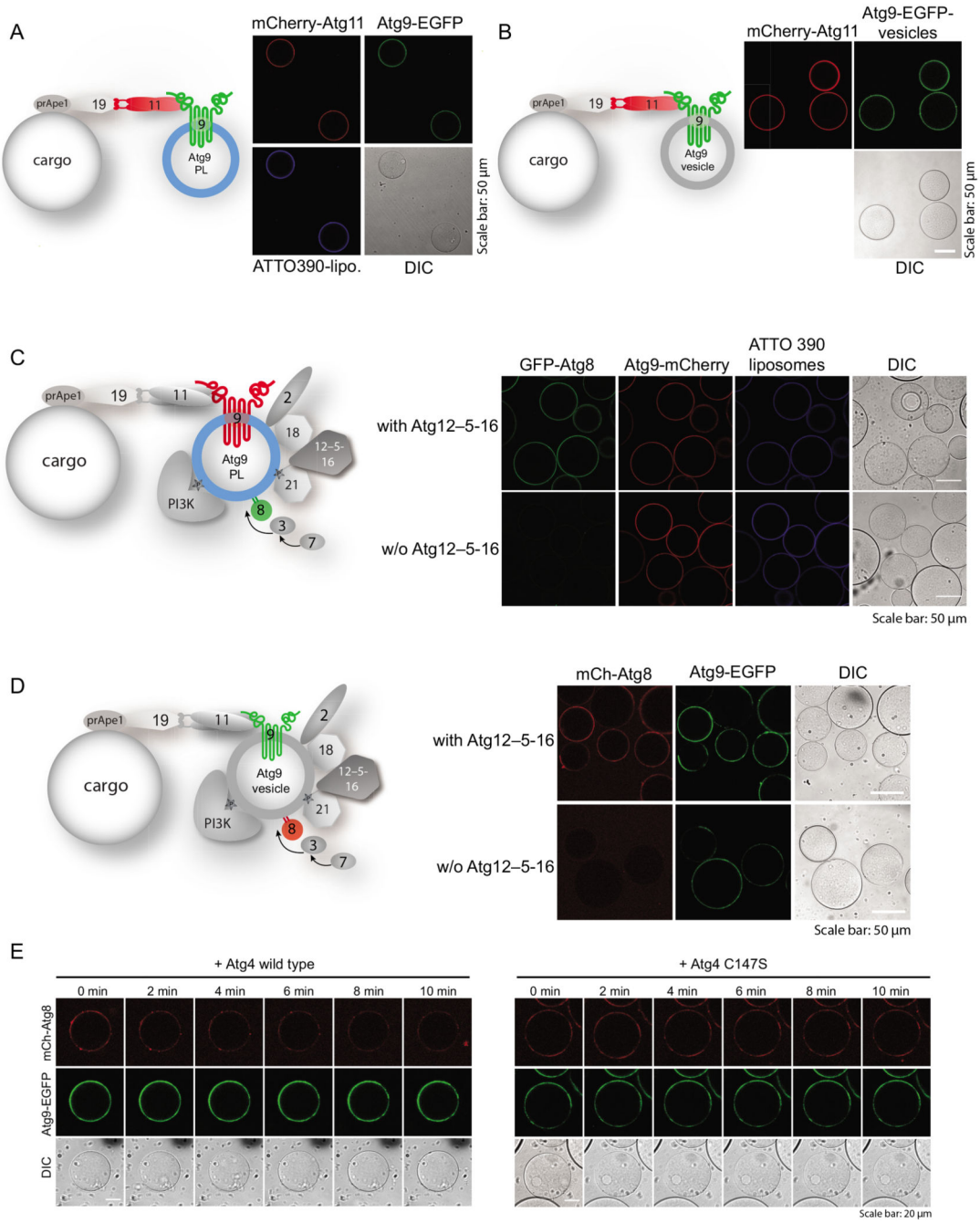

Figure 3. Reconstitution of cargo directed Atg8-lipidation to Atg9 PLs and Atg9 endogenous vesicles.

(**A, B**) Recruitment of Atg PLs and endogenous Atg9 vesicles to the cargo. Cargo mimetic beads (glutathione-sepharose) were prepared by coating with GST-prApe1 (1-41), Atg19-3D and mCherry-Atg11. For details of the pulldown see Figure S8A. The pre-assembled cargo mimetic beads were subsequently incubated with either Atg9-EGFP PLs (A) or endogenous Atg9-EGFP vesicles (B), washed and imaged. Microscopy images of representative beads are shown. The Atg9-eGFP PLs were additionally labelled with ATTO390-PE. The

experimental setup is shown by the accompanying cartoons. (**C, D**) Atg8-lipidation on the Atg9 PLs (C) and endogenous Atg9 vesicles (D) bound to the cargo mimetic beads. Glutathione sepharose beads were coated with GST-prApe1 (1-41), Atg19-3D and Atg11, incubated with Atg9-mCherry PLs (C) or Atg9-EGFP vesicles (D), washed with buffer and incubated with PI3KC3-C1, ATP, Atg21, Atg2-Atg18, Atg3, Atg12–Atg5-Atg16, eGFP-Atg8ΔR117 (C) or mCherry-Atg8ΔR117 (D) and with or without Atg12–Atg5-Atg16 (see cartoons for the experimental set-up). Microscopy images of representative beads are shown. (**E**) Time course experiment of the Atg8-deconjugation reaction on Atg9-vesicles. Atg4 wild type or the Atg4 C147S inactive mutant were added to the beads as in (D). Microscopy images were taken at the indicated time points after the addition of Atg4.

Europe PMC Funders Author Manuscripts

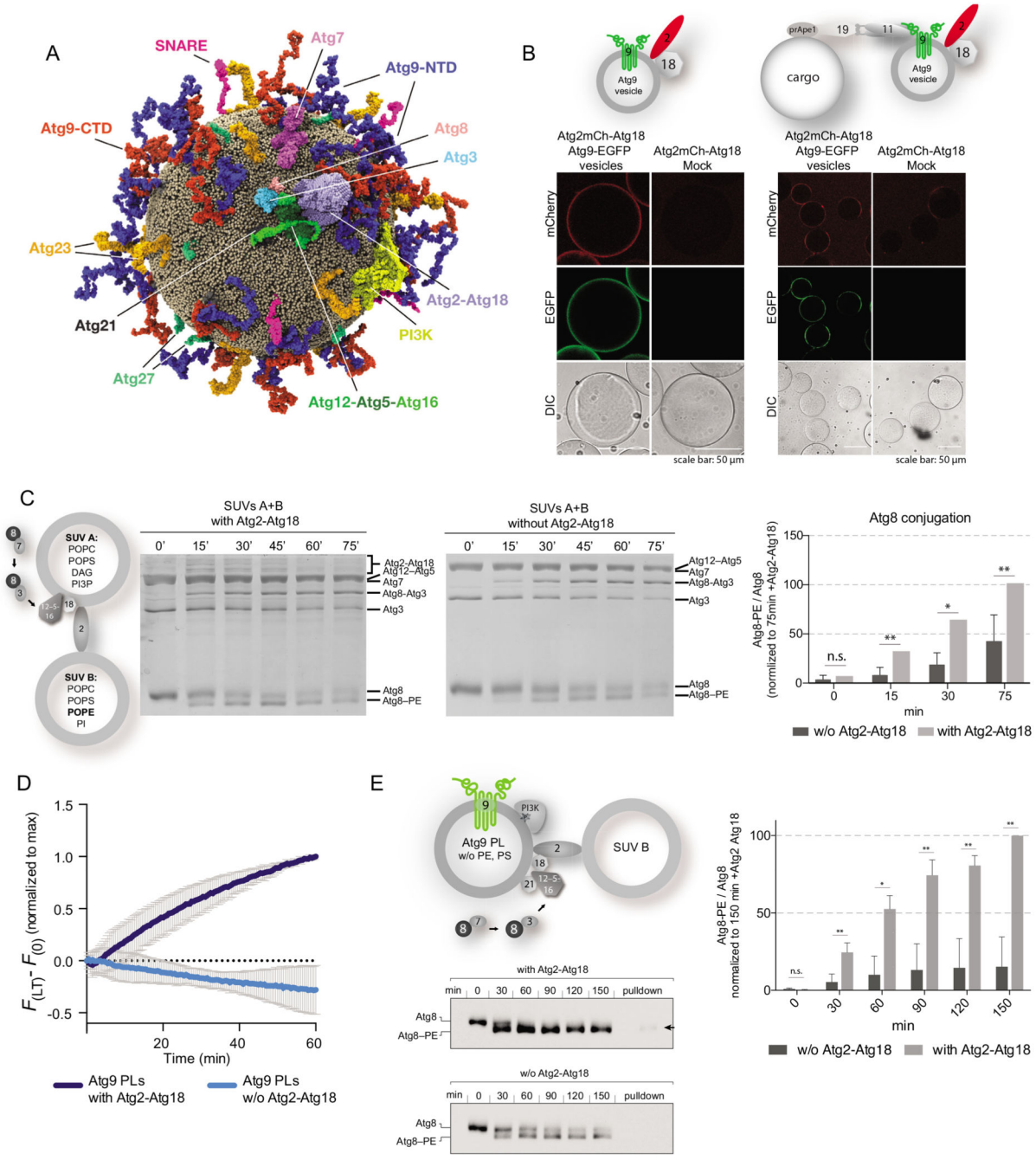

Figure 4. Atg2-mediated lipid transfer into Atg9 PLs

(**A**) Molecular model of an endogenous Atg9 vesicle. The model contains the following proteins (copy numbers in parentheses): Atg9 (28), Atg27 (10), Atg23 (10), SNAREs: SFT1 (1), TLG1 (1), VTI1 (1), SSO1 (1), GOS1 (1). Copy numbers are based on literature and mass spectrometry analysis of isolated Atg9 vesicles (see main text, Figure S6C and Methods section). Single copies of membrane-interacting autophagy proteins (PI3KC3-C1, Atg21, Atg2-Atg18, Atg3, Atg12–Atg5-Atg16, Atg8) were additionally positioned on the surface of the Atg9 vesicle. Atg9-NTD and Atg9-CTD indicate N-terminal and C-terminal

domains, respectively. Lipid head groups are shown as small grey spheres. (**B**) Atg2-Atg18 is recruited to Atg9 vesicles and cargo mimetic beads. GFP-Trap beads were coated with endogenous Atg9-EGFP vesicles. Glutathione sepharose beads were coated with GST-prApe1 (1-41), Atg19-3D and Atg11 and Atg9-EGFP vesicles and incubated with Atg2-mCherry-Atg18. Mock membranes were derived from a wild type yeast strain. (**C**) Coomassie-stained gels showing Atg8–PE conjugation assays using the depicted experimental set-up. Atg8–PE conjugation was detected as a band shift. Numbers above the gels indicate the time in minutes. (**D**) Phospholipid transfer assay based on the dequenching of NBD fluorescence. $F_{(LT)}$ and $F_{(0)}$ represent the NBD fluorescence intensity at each time point after and before addition of Atg2-Atg18, respectively, measured at 535 nm. Atg9 PLs were used as acceptor liposomes. Data are the mean values from five independent experiments. SD is shown. (**E**) Anti-Atg8 immunoblots showing Atg8–PE conjugation assays mediated by lipid transfer of Atg2-Atg18. The arrow indicates the Atg8 signal after pulling down Atg9-EGFP with GFP-Trap beads. (C and E) Quantification shows the averaged Atg8-PE/Atg8 ratio for each time point. Error bars represent the standard deviation. The quantification is based on four independent experiments. P-values were calculated using Student's t-test. Significance is indicated with * ($p \leq 0.05$), ** ($p \leq 0.01$) and *** ($p \leq 0.001$).

Europe PMC Funders Author Manuscripts

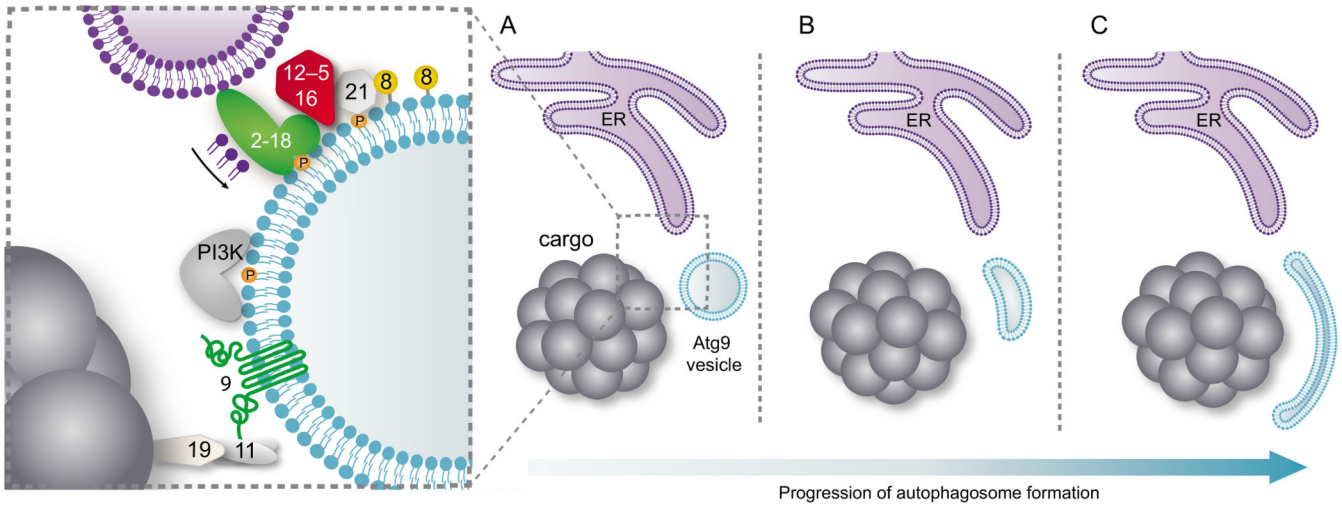

Figure 5. Model for the initial steps of the isolation membrane generation.

(**A**) Recruitment of Atg9 vesicles to the prApe1 cargo via the Atg19 receptor and Atg11 scaffold axis. The Atg9 vesicles recruit Atg2-Atg18 and PI3KC3-C1 (labelled PI3K). Production of PI3P by PI3KC3-C1 recruits Atg21 and the E3-like Atg12–Atg5-Atg16 complex. The membrane-positioned E3-like complex directs Atg8–PE conjugation to the vesicle. Atg8 lipidation is sustained by Atg2-mediated lipid transfer from a donor compartment such as the ER. (B, C) Lipid influx expands the vesicle surface resulting in isolation membrane expansion.

Europe PMC Funders Author Manuscripts